REVIEW: CLIMATOLOGY

Northern Hemisphere Ice-Sheet Influences on Global Climate Change

Peter U. Clark,[1]* Richard B. Alley,[2] David Pollard[2]

Large ice sheets actively interact with the rest of the climate system by amplifying, pacing, and potentially driving global climate change over several time scales. Direct and indirect influences of ice sheets on climate cause changes in ocean surface temperatures, ocean circulation, continental water balance, vegetation, and land-surface albedo, which in turn cause additional feedbacks in the climate system and help to synchronize global climate change. The effect of the underlying geological substrate on ice-sheet dynamics may be the missing link in understanding the ice sheet–climate interactions that are integral to the middle Pleistocene transition; the 100,000-year climate cycle; high-amplitude, millennial-scale climate variability; and low–aspect ratio ice sheets of the Last Glacial Maximum.

Following a long-term global cooling trend through much of the Cenozoic, large ice sheets first developed in the Northern Hemisphere ~2.54 million years ago (Ma) (Fig. 1) (*1, 2*). Statistical analyses of paleoclimate data support the Milankovitch theory of glaciation driven by orbital changes by showing that Northern Hemisphere ice sheets have waxed and waned with the same periods [100, 41, and 23 thousand years (ky)] as the orbital parameters (eccentricity, obliquity, precession) that control the seasonal distribution of insolation at high northern latitudes (*3*). Other features of the climate system also show these orbital periodicities, but many lag insolation forcing of climate change at high northern latitudes by much longer (5 to 15 ky, depending on the period) than expected (*4, 5*). Because ice sheets are one of the few components of the climate system with a time constant of this length, they may have been responsible for amplifying and transmitting changes that correspond to orbital periodicities in high-latitude seasonality elsewhere through the climate system with a phase lag corresponding to their long time constant (*4, 5*). According to this hypothesis, interactions among Northern Hemisphere ice sheets and other features of the climate system thus translate high-latitude insolation forcing into a global climate signal with dominant orbital-scale glaciation cycles (10^4 to 10^5 years) (*4, 5*) in which millennial-scale variations (10^3 to 10^4 years) are embedded (*6*) (Fig. 1).

Despite the success of the Milankovitch theory in explaining many aspects of the temporal and spatial variability of late Cenozoic climate change, several questions about ice sheet–climate interactions remain (Fig. 1). What are the mechanisms that nearly synchronize the climate of the Northern and Southern Hemispheres at orbital time scales despite asynchronous insolation forcing? What is the origin of the transition in variability of the global ice volume in the middle Pleistocene ~1.2 Ma, from dominant 41-ky cycles to dominant 100-ky cycles, in the absence of any change in insolation forcing? What is the origin of the dominant 100-ky cycle in the absence of any substantive insolation forcing at this period? What mechanisms are responsible for suborbital, millennial-scale climate variability? What processes caused the ice sheets of the Last Glacial Maximum (LGM) 21,000 years ago (21 ka) to be surprisingly thin and thus to have a different influence on climate than thicker ice sheets would have had?

We address these issues by first discussing mechanisms by which ice sheets can influence global climate and cause near-synchronous climate change in the polar hemispheres. We then review evidence that the dynamics of modern and former ice sheets are strongly influenced by the geological and topographic characteristics of the substrate on which the ice sheets rest. We propose that the effect of the substrate underlying the Northern Hemisphere ice sheets is to modulate ice-sheet response to insolation forcing.

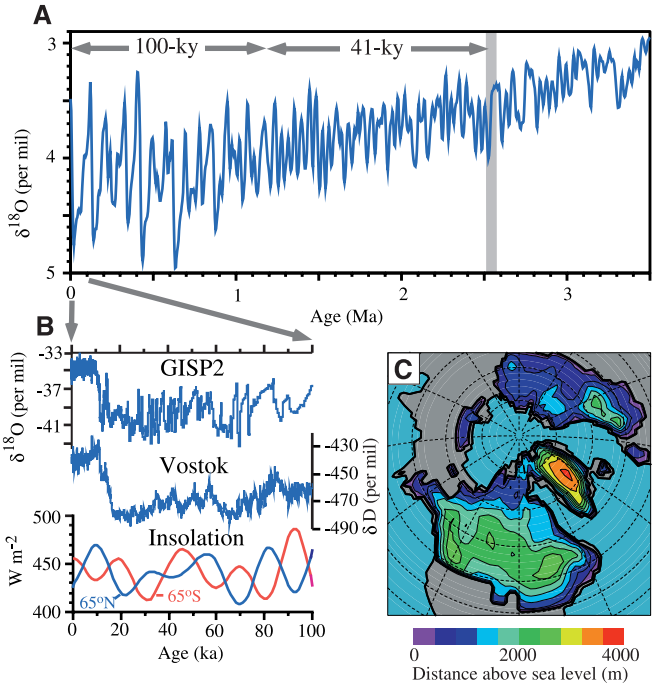

Fig. 1. (**A**) The marine $\delta^{18}O$ record [$\delta^{18}O = \{[(^{18}O/^{16}O)/(^{18}O/^{16}O)_{std}] - 1\} \times 1000$, where std is the standard mean ocean water (SMOW) reference] as a proxy for changes in (largely) global ice volume over the past 3.5 My (*2*). (**B**) The $\delta^{18}O$ record over the past 100 ky from the Greenland Ice Sheet Project 2 (GISP2) ice core (*99*), which records primarily air temperature changes over the Greenland Ice Sheet (*100*), compared with the Vostok δD (deuterium isotopic) record, which records air temperature over central Antarctica (*39*), and with midmonth insolation at 65°N for July and at 65°S for January (*101*). (**C**) Topography of the Northern Hemisphere ice sheets of the LGM 21 ka as reconstructed by the ICE-4G model (in meters above sea level) (*86*). These figures illustrate some of the issues of ice-sheet–climate interactions discussed in the text, including (A) the cause of the transition in the middle Pleistocene ~1.2 Ma, from dominant 41-ky glaciation cycles to dominant 100-ky glaciation cycles, which occurred in the absence of any substantial change in climate forcing, (B) the role of ice sheets in millennial-scale climate variability that is embedded in orbital-scale climate change, and (C) the anomalously thin Northern Hemisphere ice sheets during the LGM, which have a different effect on climate than thicker and higher ice sheets (*9, 10*).

[1]Department of Geosciences, Oregon State University, Corvallis, OR 97331, USA. [2]Environment Institute and Department of Geosciences, Pennsylvania State University, University Park, PA 16802, USA.

*To whom correspondence author be addressed. E-mail: clarkp@ucs.orst.edu

These modulated responses are then transmitted as a global climate signal through the effects of ice sheets on climate and may explain several of the key issues surrounding the evolution and behavior of the climate system over the past 2.5 Ma.

Influence of Ice Sheets on Climate

Ice sheets influence climate because they are among the largest topographic features on the planet, create some of the largest regional anomalies in albedo and radiation balance, and represent the largest readily exchangeable reservoir of fresh water on Earth. Variations in freshwater fluxes from ice sheets are especially large, because although ice sheets grow at the usually slow rate of snowfall, they shrink at the faster rate of surface melting, or the even faster rate of ice-sheet dynamics (surging). As they grow and shrink, ice sheets reorganize continental drainage by damming rivers or reversing river flow through isostatic bedrock depression under the ice, creating lakes that fill over years to centuries but that may drain an order or orders of magnitude faster when ice dams fail (*7*).

Experiments with climate models suggest several mechanisms by which Northern Hemisphere ice sheets may have influenced climate. Features of ice sheet–atmosphere interactions that are common to a number of model simulations include southward displacement of the winter jet stream by high ice sheets, substantial cooling over and downwind of the ice sheets (Fig. 2), reorganization and strengthening of storm tracks along the southern margin of the Laurentide Ice Sheet and across the North Atlantic region, and generation of large anticyclones at the ice-sheet surface (*8–11*). Circulation effects depend on the height of the ice sheet, whereas the generalized temperature effect depends primarily on ice-sheet area (*12*). For the Laurentide Ice Sheet, these effects are transmitted through the atmosphere downwind to the adjacent North Atlantic Ocean, causing a reduction in sea surface temperatures (SSTs) and an expansion of sea ice (*8, 11*).

Several dynamical ocean models indicate that the strength of the thermohaline circulation in the North Atlantic Ocean, which transfers substantial heat to high northern latitudes, is sensitive to the freshwater budget at the sites of formation of North Atlantic Deep Water (NADW) (*13–15*). Circum–North Atlantic ice sheets (Fig. 1C) are a major regulator of NADW formation and associated heat transport (*11, 16, 17*), because they affect the freshwater budget of the North Atlantic directly through release of meltwater and icebergs and indirectly through atmospheric controls on precipitation and evaporation over the North Atlantic (Fig. 2). The inherent asymmetry in the rates of ice-sheet processes—slow buildup but rapid decay and slow filling of ice-marginal lakes but rapid drainage in outburst floods—can cause orders-of-magnitude changes in freshwater fluxes.

Transmission of ice-sheet influences to North Atlantic SSTs and NADW formation would be rapid, suggesting that the North Atlantic is tightly coupled to the Northern Hemisphere ice sheets (*18*). Changes in NADW formation likely also occur through other, as yet undetermined, mechanisms, but ice sheets appear to amplify these processes (*19*). In any event, ice-sheet forcing is a well-understood mechanism that may explain many of the past variations of NADW (*20–22*). A corollary to this argument is that substantial changes in the North Atlantic system

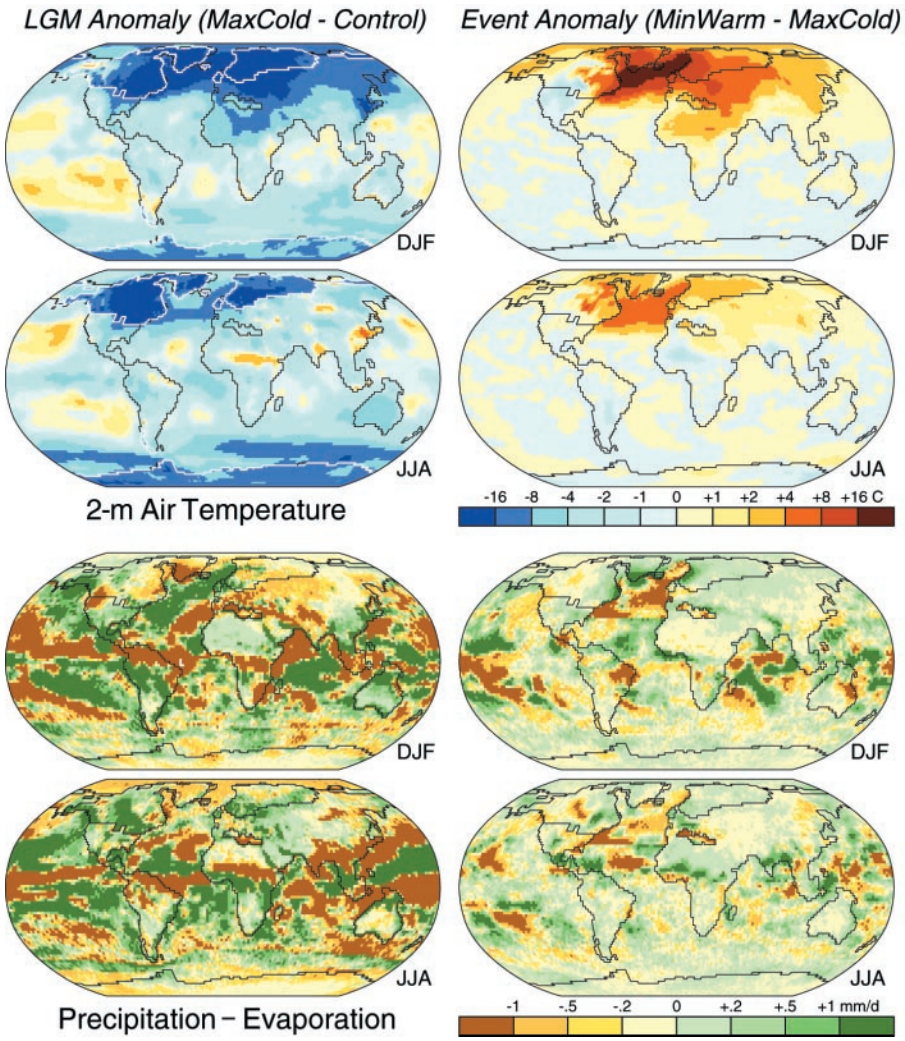

Fig. 2. Anomalies of 2-m air temperature (upper two panels in each column) and precipitation minus evaporation (P–E) (lower two panels in each column) from simulations with the GENESIS atmospheric general circulation model (*24, 26*). The four anomalies shown in the left-hand column illustrate atmospheric responses to changes in ice sheets, CO_2, sea surface temperatures (SSTs), and orbital parameters between the Last Glacial Maximum (MaxCold) and present (Control) (*26*). These anomalies show that the largest temperature decreases are in the Northern Hemisphere over and to the east of the ice sheets (outlined in white or black) and downwind from areas of colder SSTs. Large changes in P–E in winter (DJF) include increased aridity across the Asian continent and in equatorial regions, and greater moisture to the south of the ice sheets and across the North Atlantic. Large decreases in P–E in summer (JJA) are associated with the African and Asian monsoon regions. The four anomalies shown in the right-hand column include differences between a MinWarm simulation and the simulation of the nominal 21-ka boundary conditions (MaxCold) (*24, 26*). The MinWarm simulation was the same as the MaxCold simulation except that the Laurentide Ice Sheet was lowered by ~1500 m over Hudson Bay and North Atlantic SSTs north of 30°N were increased uniformly to values three-fourths of the way between glacial and modern SSTs. These changes in boundary conditions, which may represent changes that accompany a Heinrich event (*6*), cause substantial warming over the North Atlantic and downwind across Africa and Asia. These changes also enhance the African and Asian monsoons due to the warmer continents that accompany the event, and cause a reduction in P–E over the North Atlantic. [Figure courtesy of P. J. Bartlein.]

may occur largely in response to fresh water delivered from ice sheets, accompanied by only modest changes in ice-sheet size.

Climate forcing, or its amplification, caused by the release of fresh water from ice sheets to sites of NADW formation may be transmitted to distant regions through the atmosphere and ocean (*14, 15, 23, 24*). Far from the North Atlantic, however, climate anomalies at orbital time scales are much more prominent than those arising solely from changes in North Atlantic SSTs at millennial time scales (Fig. 2), because CO_2 and ice sheets differ greatly during glacial as opposed to interglacial times but only minimally in association with meltwater forcing of North Atlantic SSTs and NADW formation at millennial time scales (*25, 26*).

Reduced NADW formation, however, contributes little toward synchronizing interhemispheric climate change. In some models, shallower and southward displacement of NADW formation during glacial maxima causes cooling at high northern latitudes through expanded North Atlantic sea ice (*11*), but the NADW formation rate and its outflow to the Southern Ocean are only slightly reduced from those of modern times (*11, 27*). In contrast, a (near) collapse of NADW formation, such as occurs when it is perturbed by a large pulse of fresh water (*14, 15, 17*), causes warming in parts of the Southern Hemisphere (Fig. 3) either by reducing cross-equatorial flow of Atlantic surface waters, which leaves heat in the South Atlantic (*14, 28*), or by stimulating southward drift to supply deepwater formation in the south (*17, 29*).

Many other atmospheric and oceanic responses to ice-induced changes provide additional feedbacks that transmit the ice-sheet signal globally and contribute to synchronizing the hemispheres. Over Eurasia, colder temperatures, increases in snow cover, and changes in vegetation type increase continental aridity and albedo and weaken the African and Asian monsoons (*10, 30, 31*) (Fig. 2), thereby reducing the export of tropical water vapor and affecting cross-equatorial heat exchange. Over much of the globe, glacial-maximum surface temperatures were lower than at present, with the largest differences over ice sheets and regions of more extensive sea ice in both hemispheres (*8–10*) (Fig. 2). Enhanced polar cooling associated with ice-albedo and other feedbacks steepens the equator-to-pole temperature gradient, causing increases in wind strength (*11, 31, 32*). Stronger winds cool the tropics by upwelling of colder waters or entrainment of colder extratropical waters, further cooling the tropics and extratropics through water-vapor feedbacks on the atmosphere (*11, 33, 34*).

Model results suggest that lowered atmospheric CO_2 concentrations are required to explain the observed magnitude and symmetry of global cooling during glaciations (*9, 27, 35*). Identifying why atmospheric CO_2 concentrations have changed is problematic, however, as is establishing the temporal relation to changes in global ice volume. Deep-sea sediment records of changes in $\delta^{13}C$ values suggest that the change in CO_2 concentrations leads sea level (global ice volume) (*36*), but the integrity of the $\delta^{13}C$ record as a measure of atmospheric CO_2 concentrations is uncertain (*37*). The interpretation of $\delta^{18}O$ values of atmospheric O_2 ($\delta^{18}O_{atm}$) in ice-core records as a proxy of sea level similarly suggests that changes in atmospheric CO_2 levels lead ice volume (*38, 39*). However, other factors may influence $\delta^{18}O_{atm}$ values (*38, 40*), and putting the ice-core chronology on the same time scale as the deep-sea $\delta^{18}O$ record of global ice volume has proven difficult (*40, 41*). Currently, the only well-dated records that best link sea level to atmospheric CO_2 concentrations are for the last deglaciation, and these suggest that the initial rise in atmospheric CO_2 concentrations lags sea-level rise by 0 to 4 ky (Fig. 4). Multiple controls on atmospheric CO_2 concentrations are likely, and ice sheets are unlikely to have controlled atmospheric CO_2 concentrations completely. However, several plausible processes exist by which ice-induced changes in sea level, temperature, windiness, dust and other factors could influence atmospheric CO_2 concentrations (*40, 42*), providing a strong feedback on ice-sheet growth and decay (*43*).

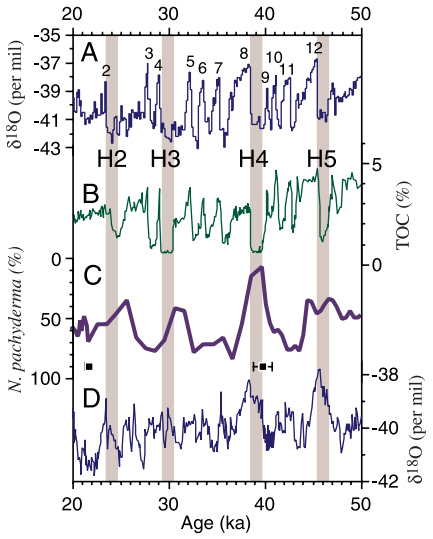

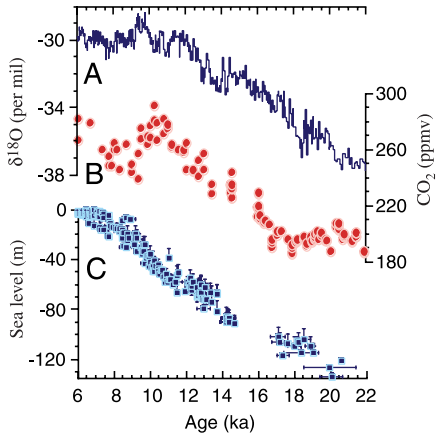

Fig. 3. (**left**) Records of millennial-scale climate variability over the interval between 20 and 50 ka from (**A**) the GISP2 $\delta^{18}O$ record (*99*), (**B**) the total organic carbon (TOC) from Arabian Sea sediments (*102*), (**C**) the percentage of *N. pachyderma* (sinistral) from core GeoB 1711 (dating control indicated by squares) (*103*) and (**D**) the $\delta^{18}O$ record from the Byrd ice core (*104*). E. J. Brook (*105*) correlated the Byrd $\delta^{18}O$ chronology to the GISP2 $\delta^{18}O$ chronology using methane data from the Byrd (*106*) and GISP2 (*107*) ice cores. There are no control points for the interval 20 to 30 ka. Dansgaard-Oeschger oscillations in the GISP2 ice core are shown as abrupt transitions separating warm interstadial climate (numbered) and cold stadial climate. Dansgaard-Oeschger oscillations are the result of changes in the rate of formation of NADW and corresponding changes in North Atlantic sea-surface temperatures (*79*). Synchronous oscillations (within dating uncertainties) in air temperature over Greenland and monsoon strength in the Arabian Sea region (increased monsoon strength during Greenland interstadials) suggest an atmospheric transmission of the North Atlantic signal to distant regions. Heinrich events H2 to H5 (shown as vertical gray bars) occur after several Dansgaard-Oeschger oscillations and during stadial events (*6*), suggesting that they may be climatically triggered (*6, 108*). Records from the South Atlantic (**C**) and parts of Antarctica (**D**) suggest a "bipolar seesaw" relationship with the North Atlantic, with a large decrease in NADW formation such as occurs during Heinrich events causing warming in parts of the Southern Hemisphere centered on the South Atlantic (*78, 79*). **Fig. 4.** (**right**) Records of changes in (**A**) $\delta^{18}O$ from the Byrd ice core, Antarctica (*109*), (**B**) atmospheric CO_2 concentrations from the Byrd core (*109*), and (**C**) eustatic sea level (*110*) during the last deglaciation. These records suggest that during the last deglaciation, the initial increase in atmospheric CO_2 concentrations lagged the initial rise in air temperatures over the Byrd region of Antarctica and the initial rise in eustatic sea level (ice-sheet melting) by 0 to 4 ky. The continental record of retreating Northern Hemisphere ice sheets (*75, 95*) suggests that sea level continued to rise during the data gap in the sea-level record shown here between ~15 and 17 ka. Interpretation of a lead-lag relation from the short record of the last deglaciation does not capture potentially different phasing relations that may be identified in longer records. However, as discussed in the text, the interpretation of longer records of various proxies of atmospheric CO_2 concentrations and sea level is subject to large uncertainties.

Ice-Sheet Dynamics

Given the importance of ice sheets in the climate system, establishing what controls their evolution and behavior is necessary to understanding their influence on climate over the past 2.5 million years (Fig. 1). This need applies equally to questions of the future

stability of the West Antarctic Ice Sheet (WAIS) (*44*). Studies of modern and former ice sheets reveal a strong connection between ice-sheet dynamics and the underlying geology (*45, 46*), suggesting that the substrate can modulate ice-sheet behavior and thus, through the influence of ice sheets on the climate system, change climate (*47–51*).

The dynamics of ice sheets that affect their size, their response time to climate change, and their release of fresh water to the oceans determine ice-sheet influences on climate. Glacial ice moves by some combination of internal ice deformation, basal sliding, and subglacial sediment deformation (*52*). If the temperature at the base of the ice sheet is below the pressure melting point, the ice is strongly coupled to the underlying substrate, and almost all motion occurs by internal ice deformation. If the temperature is at the pressure melting point, water is produced that facilitates ice motion by basal sliding and, where there is unconsolidated sediment, by sediment deformation. Compared with a frozen-bed glacier, a glacier with an unfrozen bed has a lower aspect ratio, higher balance velocity, and shorter response time, as well as other mechanisms that can generate ice-sheet instability (*47, 48*).

Unlike the relatively well-tested constitutive law for internal ice deformation, the physics of basal sliding and subglacial sediment deformation remain poorly understood *(52)*. Sliding occurs over hard bedrock (hard beds) and over unconsolidated sediments (soft beds), but it is generally favored when glacial ice is over low-friction soft beds where bed relief is low and basal water pressures are high. Subglacial sediment deformation occurs when water-saturated soft beds deform under the shear stress applied by the overlying ice sheet. The appropriate constitutive law for subglacial sediment deformation is unknown, and proposed rheologies range from slightly nonlinear (*53*) to perfectly plastic (*54*). Hindmarsh (*55*) attempted to reconcile these contrasting observations by proposing that viscous behavior at the large-scale results from multiple, distributed, small-scale failure events [see also (*56*)].

The specific processes by which soft beds influence basal motion are yet to be resolved, but we favor a general hypothesis in which basal motion is variously partitioned between sliding and subglacial sediment deformation, depending on temporal and spatial variations in subglacial hydrologic conditions and sediment properties (*57*). Conditions that result in sufficiently high basal water pressure may decouple the ice from its bed, increasing sliding at the expense of sediment deformation. Otherwise, where ice and sediment remain coupled, sediment mechanical properties, and especially their sensitivity to hydrologic variables, will control much of the movement of overlying ice. Formulating rules that describe the complex spatial and temporal variability governing basal motion—factors such as basal thermal regime, subglacial hydrology, ice-bed coupling, sediment rheology, and continuity—represents a substantial challenge to modeling the long-term behavior and evolution of ice sheets (*47, 58*).

Observations beneath the WAIS suggest that basal motion is strongly linked to substrate geology. Basal motion is responsible for the presence of fast-flowing ice streams in WAIS [velocities of 10^2 to 10^3 meters per year (m/year)], which are confined on either side by slow-moving sheet flow (10^0 to 10^1 m/year) and account for nearly all the discharge of WAIS (*59*), as well as for the low-aspect ratio of the ice sheet (*46*). Geophysical observations (*60*) and drilling (*61*) have shown that several WAIS ice streams draining into the Ross Sea are underlain by soft beds with basal water pressures that nearly cause ice flotation. The head of one of these ice streams coincides with the upstream edge of a sedimentary basin, suggesting that the presence of ice streaming is determined by the presence of sedimentary basins (*50*).

Geological evidence from the areas covered by former Northern Hemisphere ice sheets also suggests a strong relation between the distribution of soft beds and enhanced basal flow (*45, 49*). Both the Laurentide and Fennoscandian Ice Sheets have central areas of sedimentary basins that are largely below sea level at present (Hudson Bay, Gulf of Bothnia) and were even lower when depressed by the weight of the ice sheets. These core areas are surrounded by crystalline bedrock, which in turn is surrounded by sedimentary bedrock. Areas of sedimentary bedrock typically have low relief and are covered by relatively continuous, low-permeability unconsolidated sediments, suggesting that these soft-bedded areas would be predisposed to fast ice flow when basal motion is activated (*62*) (Fig. 5). In contrast, the higher relief and discontinuous sediment cover characteristic of crystalline bedrock areas suggest stronger ice-bed coupling and thus reduced ice flow (*62*) (Fig. 5).

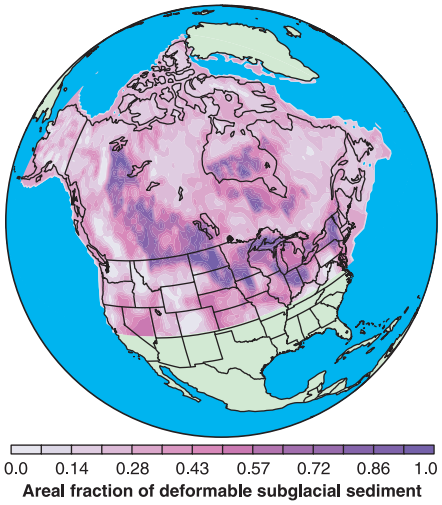

Fig. 5. Areal fraction of deformable subglacial sediment for the area covered by the Laurentide Ice Sheet. Area of deformable sediment cover is determined by digitizing the fraction of glacial sediments in 1° × 1° longitude-latitude cells, based on surficial-geologic maps (*62*). [Figure courtesy of S. J. Marshall.]

Middle Pleistocene Transition

At the middle Pleistocene transition ~1.2 Ma, the dominant 41-ky ice-volume variations changed to dominant 100-ky variations under essentially the same orbital forcing (*63*) (Fig. 6). The transition is also seen in records of those features of the climate system that are driven by ice sheets (*64–67*) (Fig. 7), suggesting that the mechanism responsible for the transition in ice-sheet size and variability ultimately was responsible for a substantial change in the behavior of the climate system.

Ice sheet–climate models that have been used to explore the cause of the middle Pleistocene transition produce a transition as a nonlinear response either to a prescribed, long-term cooling trend associated with de-

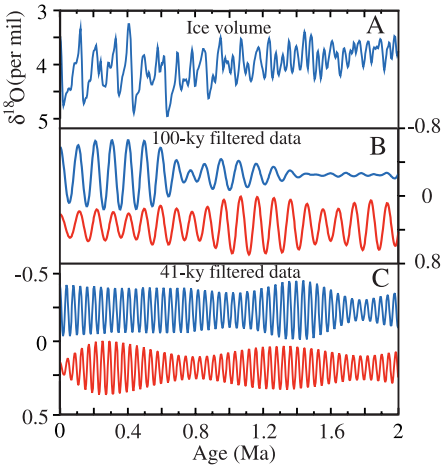

Fig. 6. (**A**) Marine $\delta^{18}O$ record of global ice volume from Ocean Drilling Program (ODP) Site 849 over the past 2 My (*2*). (**B**) Blue curve is the filtered $\delta^{18}O$ record in (A) using a 100-ky filter [in per mil and offset from scale in (A)]. Red curve is the filtered eccentricity index from (*111*) obtained by using the same filter as used for the isotope data (arbitrary scale). (**C**) Blue curve is the filtered $\delta^{18}O$ record in (A) obtained by using a 41-ky filter [in per mil and offset from scale in (A)]. Red curve is the filtered obliquity index from (*111*) obtained by using the same filter as used for the isotope data (arbitrary scale). Note the onset of large-amplitude 100-ky ice-volume cycles at ~1.2 Ma (middle Pleistocene transition), during which time the amplitude of the 100-ky eccentricity cycles decreases and the amplitude of the 41-ky obliquity does not change. [Figure courtesy of A. C. Mix.]

creasing atmospheric CO_2 concentrations (*68, 69*) or to a suddenly imposed switch in model physics (*70*). Data constraining a long-term cooling trend or a decrease in atmospheric CO_2 concentrations over the past 3 million years are lacking, but these models suggest that such a trend is a possible cause of the transition.

Geologic records indicate that the Laurentide Ice Sheet, which dominates the global ice volume signal, was more areally extensive before the transition than after (*51*). In contrast, the $\delta^{18}O$ record of global ice volume indicates a large increase in ice volume after the transition (Fig. 6). These apparently contradictory records can be reconciled by invoking a change at the transition from thinner (~2 km) to thicker (~3 km) ice sheets, which requires a change in the basal flow condition. At the inception of Northern Hemisphere glaciation, hard-bedded areas were covered by a thick (tens of meters), deeply weathered soil (regolith) that built up in northern latitudes over tens of millions of years before the growth of the ice sheets. This widespread soft bed can maintain relatively thin, low-volume ice sheets, which respond linearly to the dominant (~21- and 41-ky) orbital forcing (*51*). Glacial erosion of the regolith and resulting exposure of crystalline bedrock, therefore, may have allowed ice-sheet thicknesses and bedrock depressions to become large enough to introduce mechanisms responsible for the dominant nonlinear ~100-ky response to orbital forcing over the past 1.2 Ma (Fig. 6) (*51*).

The 100-ky Cycle

Although the main periodicities of the deep-sea $\delta^{18}O$ record of global ice volume (100, 41, and 23 ky) are the same as those that dominate orbital changes in insolation, ice-volume changes show a linear response only to obliquity and precession (*4*). In contrast, the effect of eccentricity variations (~100 ky and longer) on insolation is to modulate the amplitude of the precession variations (~23 and 19 ky), so the resulting 100-ky amplitude in variations in insolation forcing is much too small to explain the large ice-volume response at this period (*5*). This suggests either that the response of ice sheets to the orbital forcing is nonlinear or that some internal climate oscillation is either phase locked to orbital forcing or has an independent phase [reviewed in (*5*)] (*71*). In either case, ice sheets no longer respond directly to orbital forcing, but through their influence on the climate system, they become the primary mechanism responsible for driving the 100-ky climate cycle (Fig. 7).

The 100-ky cycle is, in most cases, asymmetric, with long (~90-ky), fluctuating growth phases and rapid (~10-ky) terminations (*72*) (Fig. 8). In contrast to the smaller ice sheets that prevailed before 1.2 Ma and responded linearly to insolation forcing, the large 100-ky ice sheets required some instability to trigger deglaciation (*5, 51*). Many model results suggest that precession and obliquity forcing cause ice sheets to grow to some critical size beyond which they no longer respond linearly to orbital forcing; deglaciation then occurs through nonlinear interactions between the ice sheets, oceans, and lithosphere. These interactions can develop once some threshold is exceeded (*5*) that permits deglaciation to be triggered by the next Northern Hemisphere summer insolation maximum. The statistical linkage of the 100-ky cycle to that of eccentricity suggests that eccentricity may have a role in triggering deglaciation through its modulation of the precession cycle (*3*). Any model of the 100-ky cycle, however, must explain why the ice sheets no longer responded in a completely linear fashion to orbital forcing after the middle Pleistocene transition, as well as the mechanism or mechanisms for rapid deglaciation.

Did soft beds play a role in the amplification of the 100-ky cycle? Modeling results indicate that widespread soft beds maintain thin ice sheets, which respond linearly to insolation forcing, whereas widespread hard beds allow the growth of thicker ice sheets that require mechanisms for deglaciation that are nonlinear (*51*). The Laurentide and Fennoscandian Ice Sheets, however, rested on extensive marginal areas of soft beds when they were at their maximum extents (Fig. 5). No models have explored the role that soft beds may have played in causing terminations, but several existing models of the 100-ky cycle require fast ice flow for deglaciation (*73, 74*), suggesting that soft beds, by enabling fast basal motion, may be involved.

We evaluate the relation between the timing of ice-sheet advance onto the outer soft-bedded zones (Fig. 5) and 100-ky cycles by identifying the point on the $\delta^{18}O$ global ice volume (sea-level) curve where the Laurentide and Fennoscandian Ice Sheets grow large enough to extend onto marginal soft-bedded regions (Fig. 8). This relation suggests that

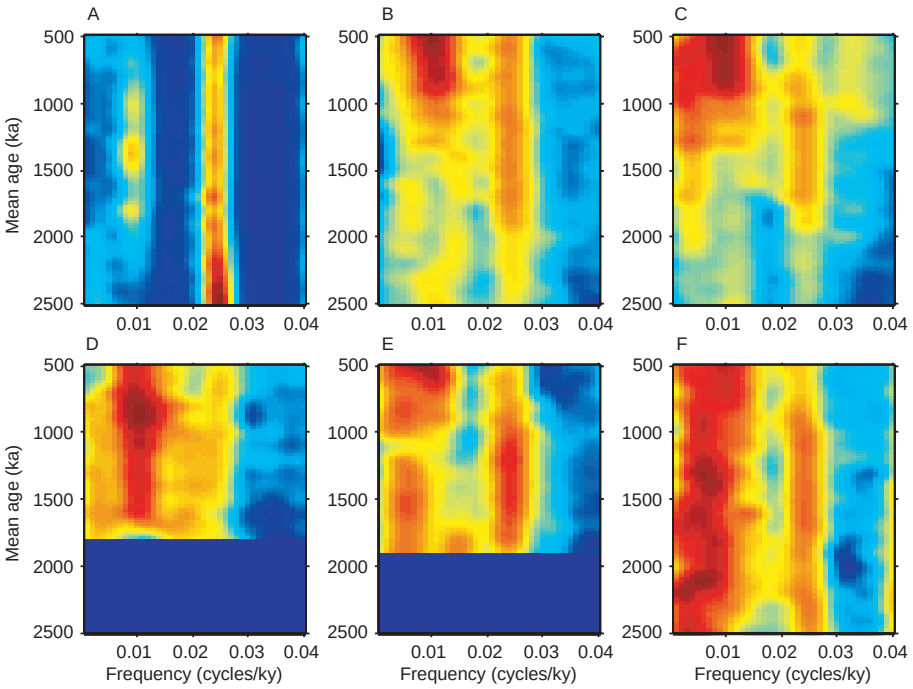

Fig. 7. Evolutive spectra (*112*) for (**A**) variations in eccentricity and tilt (*101*), (**B**) $\delta^{18}O$ (per mil) from ODP Site 849 in the Pacific Ocean (*2*), (**C**) $\delta^{13}C$ (per mil) from Deep Sea Drilling Project (DSDP) Site 607 in the North Atlantic (*21*), (**D**) the percent biogenic silica from Lake Baikal (*65*), (**E**) the grain size ratio of <2 μm to >10 μm from Chinese loess (*67*), and (**F**) the percent lithogenic detritus from ODP Site 722 in the northwest Arabian Sea (*66*). Variance is expressed as a logarithm for all figures except (A), which is plotted on a linear scale. Red colors are high values of variance, lighter blues are low values, and dark blue areas on (D) and (E) are no data. These data suggest that growth and decay of ice sheets influenced the rate of formation of NADW (C) (*21*), temperatures and aridity of northern and eastern Africa (*64*) and Asia (D, E) (*65–67*), the East Asian winter monsoon (*67*), and the Asian summer monsoon (*66*). Before the onset of Northern Hemisphere glaciation ~2.54 Ma, Asian temperature and hydrology and low-latitude monsoonal climate were responding to regional precessional and obliquity forcing. After 2.5 Ma, changes in Asian and African climate became largely in phase with or lagged changes in the ice sheets (*64–67*), indicating that they are now driven largely by the ice sheets through their influence on the atmosphere. A substantial increase in 100-ky variance in these proxies after the middle Pleistocene transition in association with the onset of large 100-ky ice-sheet cycles further identifies these ice sheet–climate relations. [Figure courtesy of N. G. Pisias.]

orbital forcing causes both ice sheets to grow to a large size on intermediate hard-bedded regions, possibly modulated by the influence of an inner core of soft beds (*48*). The ice sheets, however, only advance onto the outer zone of soft beds late in a 100-ky glaciation cycle (*75*), after which they are followed by major terminations (I, II, IV, V, and VII) (Fig. 8). Because this relation indicates that only the largest ice sheets advance onto soft beds, it is consistent with those models of the 100-ky cycle that invoke runaway deglaciations only after the ice sheets attain a threshold thickness and volume. We thus propose that the growth of 100-ky ice sheets onto the outer soft beds combines with other key feedback processes such as sea-level changes (*5*) and glacial isostasy (*76*) to cause the abrupt terminations of the 100-ky cycles. Soft beds may have been deeply frozen in many areas when ice sheets first advanced onto them, although some areas, such as in existing lake basins, may have been unfrozen from the outset. The long time scale of permafrost response to the insulation provided by the overlying ice sheet (order of 10^3 to 10^4 years) (*77*) would allow the ice sheets to maintain steep profiles and high surface elevations after they first advanced over the frozen soft beds. Subsequent thawing of permafrost by geothermal heat flow beneath the ice sheets would enable fast ice discharge to low (warmer) elevations and to the adjacent oceans and lakes, where rapid ablation would occur (*9, 47, 48*). The result may be an ice stream–dominated, West Antarctic–type ice sheet, with a substantially reduced response time to climate changes, and thus with the ability to be lowered further and to deglaciate more rapidly during the next rise in Northern Hemisphere insolation that brings warmer summers and ice retreat.

Millennial Time Scales

Millennial-scale (10^3-year) climate variations are too short and frequent to be explained by orbital forcing, but Northern Hemisphere ice sheets clearly play a role that, in many ways, may parallel their role in climate change at orbital time scales (Fig. 2). In particular, ice sheets force or amplify large, abrupt, and widespread millennial-scale climate changes through the release of fresh water to the North Atlantic, causing changes in SSTs and in NADW formation that are transmitted through the atmosphere and the ocean with various feedbacks amplifying and further transmitting the signal regionally or globally (*23, 24, 78, 79*) (Figs. 2 and 3).

The two dominant modes of millennial-scale climate variability during glaciations are Dansgaard-Oeschger (D/O) cycles, with an approximate spacing of 1500 years, and Heinrich events, which have, by comparison, a long and variable spacing (10^3 to 10^4 years) (Fig. 3) (*6, 19*). The D/O oscillation is an oceanic process, often triggered by meltwater changes (*22, 25, 80*) but possibly also oscillating freely as stochastic variability (*17*) or in response to an El Niño–Southern Oscillation–type mechanism (*81*). D/O climate change is centered on the North Atlantic and on regions with strong atmospheric response to changes in the North Atlantic (Figs. 2 and 3).

Most Heinrich events involve surging of the Laurentide Ice Sheet through the Hudson Strait, apparently triggered by D/O cooling (*6, 19*). The icebergs released to the North Atlantic during a Heinrich event cause a near shutdown in the formation of NADW (*82*). In addition to the atmospheric transmission seen for D/O oscillations, Heinrich events are also transmitted elsewhere through the ocean (*17, 78, 79*) (Fig. 3).

Soft beds provide a mechanism for millennial-scale ice-sheet behavior. Routing of meltwater along the southern margin of the Laurentide Ice Sheet to the North Atlantic was regulated by the rapid advance and retreat of surge lobes over marginal areas of soft beds (Fig. 5), and changes in this routing apparently triggered some abrupt climate changes (*49, 80*). Heinrich events involve an instability of ice dynamics that is readily modeled by incorporating soft beds in the Hudson Bay and Hudson Strait (Fig. 5) (*48, 83*).

Ice Sheets at the Last Glacial Maximum

The LGM (21 ka) is a critical period for understanding climate dynamics, because LGM climate is relatively well-constrained by paleoclimate data that provide boundary conditions for climate models and permit an evaluation of model performance (*84*). A number of important issues in LGM climate remain unresolved (*85*), however, including the thickness of the Northern Hemisphere ice sheets. Geophysical (Earth) models using crustal rebound and associated relative sea-level change (*86, 87*) reconstruct ice sheets that are 1000 to 2000 m thinner than those reconstructed by ice-sheet models, which include ice flow by internal ice deformation and basal sliding only (*74, 88, 89*) (Figs. 1 and 9). A novel proposal using a nonstandard ice rheology that is 20 times as soft at low stresses as in traditional models would produce the reconstructed thin ice sheets (*74, 76*). However, ice-texture data raise questions about the applicability of this proposed ice rheology to more rapidly deforming ice that largely controls ice-sheet form (*90*). Ice-shelf spreading is well-described by the accepted rheology (*91*), and this solution to the low-aspect-ratio problem does not yet account for the evidence for basal lubrication in marginal regions of former ice sheets (*45, 49*).

Ice-sheet models that introduce the effects of soft beds (*92–94*) successfully reproduce the low–aspect ratio Laurentide Ice Sheet reconstructed by Earth models that use relative sea-level data (Fig. 1), suggesting that soft beds provide a reasonable mechanism to explain the shape and volume of the ice sheet that is consistent with observations of relative sea-level change and other geodynamic considerations. Sensitivity studies show, however, that thick LGM ice over Hudson Bay as

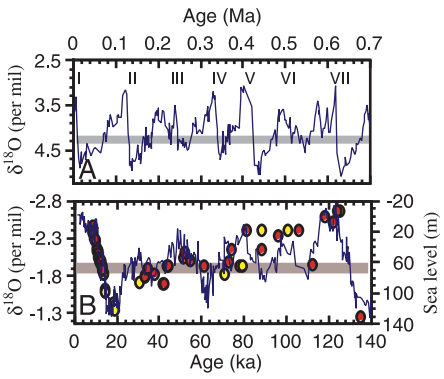

Fig. 8. (**A**) Marine $\delta^{18}O$ record of global ice volume from ODP Site 849 over the past 0.7 Ma (*2*). Terminations I to VII (*72*) are labeled across the top of the isotope record. The horizontal gray bar represents the point on the isotope record when the retreating margins of both the Laurentide and Fennoscandian Ice Sheets were last at the contact between the hard-bedded and outer soft-bedded zones ~13 calendar ka (11 ^{14}C ka) (*49*). We use this point to establish those times before the last deglaciation when the ice-sheet margins advanced beyond the hard-bedded zone onto the outer soft-bedded zone (that is, $\delta^{18}O$ values were more positive than the value where the bar intersects the $\delta^{18}O$ scale). The absence of major deglaciations at terminations III and VI coincides with times when the ice sheets did not reach large sizes and thus remained largely on hard beds. (**B**) Marine $\delta^{18}O$ record of global ice volume over the past 140 ka from ODP Site 769 in the Sulu Sea (blue line) (*113*) compared with estimates of past sea level from raised corals (dated by U/Th and corrected for tectonic uplift). Red dots are samples from New Guinea (*114*), and yellow dots are samples from Barbados (*115*). The horizontal gray bar is fixed on the $\delta^{18}O$ axis in the same way as described in (A). The isotope record closely matches the coral record, suggesting that the Sulu Sea isotope record is primarily one of global ice volume (*113*). Comparing this isotope record with the one from Site 849 in (A) suggests that the latter record also has a strong temperature signal during marine isotope stage 3. The only important time that the ice sheets advanced onto the outer zone of soft beds during the last glaciation was thus during isotope stage 2, consistent with the continental record of the last glaciation (*75*). If the earlier (before 125 ka) part of the Site 849 isotope record overestimates ice volume in a similar way, then the ice sheets may similarly have only advanced onto the outer zone of soft beds during only the latest times of major glaciation cycles.

reconstructed in the Earth models is only possible if the soft beds in that region are deactivated, whereas soft beds underlying the outer periphery of the ice sheet are active (*93, 94*). Moreover, a progressive reduction in the effect of these outer soft beds on ice flow causes the Laurentide Ice Sheet to change from an asymmetrical, multidomed, low-elevation geometry (for example, Fig. 1) toward a symmetrical, centrally domed, high-elevation form (Fig. 9A) (*95*). Because there are uncertainties in whether isostatic equilibrium was achieved at the LGM and in the specific properties of lower-mantle viscosity, LGM ice sheets may have been thicker and higher than reconstructed in current Earth models (*96*). Thicker and higher LGM ice sheets are made possible by deactivating soft-bedded areas, which may occur by increasing the fraction of the bed that is frozen (*93, 95*). As discussed above, reactivating large regions of soft beds may have precipitated not only thinner ice sheets near the LGM but also the rapid deglaciation that caused the 100-ky cycle.

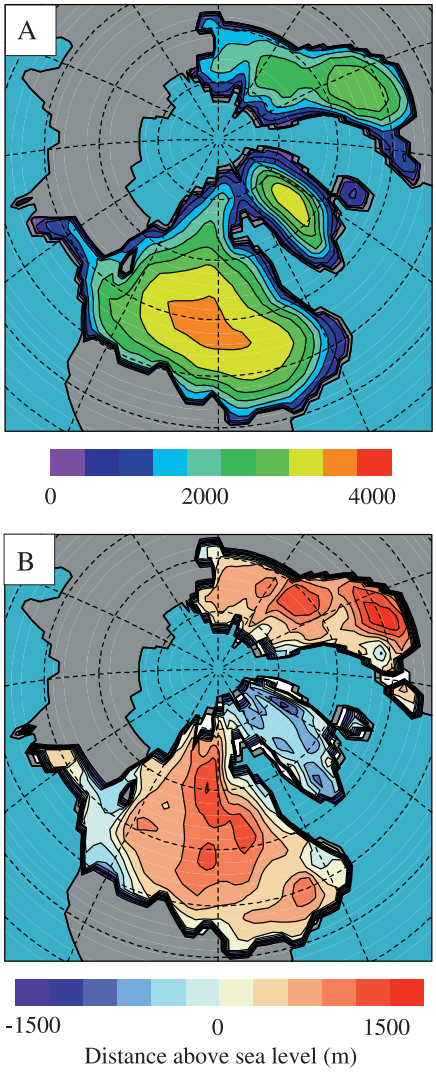

Fig. 9. (**A**) Topography of the Northern Hemisphere ice sheets during the LGM 21 ka reconstructed by the CLIMAP Project Members (scale in meters above sea level) (*88*). (**B**) The difference in topography between the CLIMAP and ICE-4G reconstructions (scale in meters above sea level), showing that ice sheets in the ICE-4G model (see Fig. 1) are substantially thinner (lower aspect ratios) than those reconstructed by CLIMAP. From (*9*).

Discussion

Climate model simulations and climate records demonstrate the importance of ice sheets in modulating late Cenozoic climate variability both directly through topographic and ice-albedo forcing and indirectly through sea-level changes and freshwater discharge. On orbital time scales, ice sheets have contributed to (near) synchronization of interhemispheric climate change. Smaller and faster ice-sheet changes caused regional to hemispheric or broader atmospheric responses and, where transmitted through the deep ocean, an antiphase response centered on and downwind of the South Atlantic. Interpretation of climate records should be viewed as the superposition of climate variability at these different time scales, particularly during glacial to interglacial transitions when changes occurring at both millennial and orbital time scales are large (*25*).

Long paleoclimate records also demonstrate that, at orbital time scales, several features of the climate system at low and southern latitudes respond to high northern latitude insolation forcing but at an earlier phase than the response of Northern Hemisphere ice sheets (*4, 5, 97*). To what extent these early responses may influence ice sheets remains an important question. Similarly, many parts of the climate system that do respond to ice-volume changes also respond to regional insolation forcing (*66, 98*), and these regional responses may also provide important feedbacks to ice-sheet growth and decay.

The influence of soft beds on ice-sheet dynamics has emerged as an important concept in understanding the behavior of WAIS (*44, 46, 50*). The geological record suggests that soft beds also influenced former Northern Hemisphere ice sheets, and we propose that geologically modulated ice-sheet behavior may explain several longstanding issues in late Cenozoic climate dynamics. A number of critical issues have yet to be resolved, however, before we can fully understand this substrate–ice–climate relation, ranging from a better formulation of how soft beds interact with ice sheets to further understanding how ice-sheet–atmosphere–ocean interactions influence long-term ice-sheet behavior.

References and Notes

1. N. J. Shackleton, A. Berger, W. R. Peltier, *Trans. R. Soc. Edinburgh Earth Sci.* **81**, 251 (1990).
2. A. C. Mix *et al.*, *Proc. Ocean Drill. Prog. Sci. Results* **138**, 371 (1995).
3. J. D. Hays, J. Imbrie, N. J. Shackleton, *Science* **194**, 1121 (1976); J. Imbrie *et al.*, in *Milankovitch and Climate, Part 1*, A. L. Berger *et al.*, Eds. (Kluwer Academic, Boston, MA, 1984), pp. 121–164.
4. J. Imbrie *et al.*, *Paleoceanography* **7**, 701 (1992).
5. J. Imbrie *et al.*, *Paleoceanography* **8**, 699 (1993).
6. G. Bond *et al.*, *Nature* **365**, 739 (1993).
7. J. S. Walder and J. E. Costa, *Earth Surf. Proc. Land.* **21**, 701 (1992).
8. S. Manabe and A. J. Broccoli, *J. Geophys. Res.* **90**, 2167 (1985).
9. D. Pollard and S. L. Thompson, *Quat. Sci. Rev.* **16**, 841 (1997).
10. J. Kutzbach *et al.*, *Quat. Sci. Rev.* **17**, 473 (1998).
11. A. Ganopolski, S. Rahmstorf, V. Petouknov, M. Claussen, *Nature* **391**, 351 (1998).
12. D. Rind, *J. Geophys. Res.* **92**, 4241 (1987); R. A. Shinn and E. J. Barron, *J. Clim.* **2**, 1517 (1989); B. Felzer, R. J. Oglesby, T. Webb III, D. E. Hyman, *J. Geophys. Res.* **101**, 19, 077 (1996).
13. E. Maier-Raimer and U. Mikolajewicz, in *Oceanography 1988*, A. Ayala-Castanares, W. Wooster, A. Yanez-Arancibia, Eds. (UNAM, Mexico, 1989), pp. 87–100.
14. T. F. Stocker, D. G. Wright, W. S. Broecker, *Paleoceanography* **7**, 529 (1992).
15. S. Rahmstorf, *Nature* **378**, 145 (1995).
16. W. S. Broecker, G. Bond, M. Klas, *Paleoceanography* **5**, 469 (1990); E. G. Birchfield, H. Wang, J. J. Rich, *J. Geophys. Res.* **99**, 12, 459 (1994).
17. A. J. Weaver, in *Mechanisms of Global Climate Change at Millennial Time Scales*, P. U. Clark, R. S. Webb, L. D. Keigwin, Eds. [American Geophysical Union (AGU), Washington, DC, 1999], pp. 285–300.
18. W. F. Ruddiman, in *North America and Adjacent Oceans During the Last Deglaciation*, W. F. Ruddiman and H. E. Wright, Jr., Eds. (Geological Society of America, Boulder, CO, 1987), pp.137–154.
19. G. C. Bond *et al.*, in *Mechanisms of Global Climate Change at Millennial Time Scales*, P. U. Clark, R. S. Webb, L. D. Keigwin, Eds. (AGU, Washington, DC, 1999), pp. 35–58.
20. A. C. Mix and R. G. Fairbanks, *Earth Planet Sci. Lett.* **73**, 231 (1985); E. A. Boyle and L. D. Keigwin, *Nature* **330**, 35 (1987); P. B. deMenocal, D. W. Oppo, R. G. Fairbanks, W. L. Prell, *Paleoceanography* **7**, 229 (1992).
21. M. E. Raymo, W. F. Ruddiman, N. J. Shackleton, D. W. Oppo, *Earth Planet. Sci. Lett.* **97**, 353 (1990).
22. L. D. Keigwin, G. A. Jones, S. J. Lehman, E. Boyle, *J. Geophys. Res.* **96**, 16, 811 (1991).
23. D. Rind, D. Peteet, W. S. Broecker, A. McIntyre, W. F. Ruddiman, *Clim. Dyn.* **1**, 3 (1986); P. J. Fawcett, A. M. Agustsdottir, R. B. Alley, C. A. Shuman, *Paleoceanography* **12**, 23 (1997); U. Mikolajewicz, T. J. Crowley, A. Schiller, R. Voss, *Nature* **387**, 384 (1997).
24. S. W. Hostetler, P. U. Clark, P. J. Bartlein, A. C. Mix, N. G. Pisias, *J. Geophys. Res.* **104**, 3947 (1999).
25. R. B. Alley and P. U. Clark, *Annu. Rev. Earth Planet. Sci.* **27**, 149 (1999).
26. S. W. Hostetler and P. J. Bartlein, in *Mechanisms of Global Climate Change at Millennial Time Scales*, P. U. Clark, R. S. Webb, L. D. Keigwin, Eds. (AGU, Washington, DC, 1999), pp. 313–328.
27. A. J. Weaver, M. Eby, A. J. Fanning, E. C. Wiebe, *Nature* **394**, 847 (1998).
28. A. C. Mix, W. F. Ruddiman, A. McIntyre, *Paleoceanography* **1**, 43 (1986); S. Manabe and R. J. Stouffer, *J. Clim.* **1**, 841 (1988); T. J. Crowley, *Paleoceanography* **7**, 489 (1992).
29. A. Schiller, U. Mikolajewicz, R. Voss, *Clim. Dyn.* **13**, 325 (1997).
30. W. L. Prell and J. E. Kutzbach, *J. Geophys. Res.* **82**, 8411 (1987); J. Overpeck, D. Anderson, S. Trumbore, W. Prell, *Clim. Dyn.* **12**, 213 (1996).
31. P. B. deMenocal and D. Rind, *J. Geophys. Res.* **98**, 7265 (1993).
32. J. T. Overpeck, L. C. Peterson, N. Kipp, J. Imbrie, D. Rind, *Nature* **338**, 553 (1989).
33. A. B. G. Bush and S. G. H. Philander, *Science* **279**, 1341 (1998).
34. A. Ágústsdóttir, R. B. Alley, D. Pollard, W. H. Peterson, *Geophys. Res. Lett.* **26**, 1333 (1999).
35. A. J. Broccoli and S. Manabe, *Clim. Dyn.* **1**, 87 (1987).

36. N. J. Shackleton and N. G. Pisias, in *The Carbon Cycle and Atmospheric CO_2: Natural Variations Archean to Present*, E. T. Sundquist and W. S. Broecker, Eds. (AGU, Washington, DC, 1985), pp. 303–317.
37. W. B. Curry and T. J. Crowley, *Paleoceanography* **2**, 480 (1987); H. J. Spero, J. Bijma, D. W. Lea, B. E. Bemis, *Nature* **390**, 497 (1997).
38. T. Sowers, M. Bender, D. Raynaud, Y. S. Korotkevich, J. Orchardo, *Paleoceanography* **6**, 679 (1991).
39. J. R. Petit *et al*., *Nature* **399**, 429 (1999).
40. W. S. Broecker and G. M. Henderson, *Paleoceanography* **13**, 352 (1998).
41. M. E. Raymo and M. Horowitz, *Geophys. Res. Lett*. **23**, 367 (1996).
42. W. H. Berger, *Naturwissenschaften* **69**, 87 (1982); W. S. Broecker, *The Glacial World According to Wally* (Lamont-Doherty Earth Observatory, Palisades, NY, 1995); D. A. Hodell and C. D. Charles, *Eos* **80** (17), S198 (1999).
43. Changes in atmospheric CO_2 concentrations are undoubtedly important in the climate changes of Earth history, but probably as a feedback rather than as a direct forcing in many or most cases; our understanding of CO_2-climate relations is evolving rapidly [M. Pagani, M. A. Arthur, K. H. Freeman, *Paleoceanography* **14**, 273 (1999); P. N. Pearson and M. R. Palmer, *Science* **284**, 1824 (1999)] and is beyond the scope of this review.
44. C. R. Bentley, *Science* **275**, 1077 (1997); M. Oppenheimer, *Nature* **393**, 325 (1998).
45. G. S. Boulton and A. S. Jones, *J. Glaciol*. **24**, 29 (1979).
46. R. B. Alley, D. D. Blankenship, C. R. Bentley, S. T. Rooney, *Nature* **322**, 57 (1986).
47. D. R. MacAyeal, *Nature* **359**, 29 (1992).
48. _____, *Paleoceanography* **8**, 775 (1993).
49. P. U. Clark, *Quat. Res*. **41**, 19 (1994).
50. S. Anandakrishnan, D. D. Blankenship, R. B. Alley, P. L. Stoffa, *Nature* **394**, 62 (1998); R. E. Bell *et al*., *Nature* **394**, 58 (1998).
51. P. U. Clark and D. Pollard, *Paleoceanography* **13**, 1 (1998).
52. W. S. B. Paterson, *The Physics of Glaciers* (Pergamon, Tarrytown, NY, ed. 3, 1994); R. LeB. Hooke, *Principles of Glacier Mechanics* (Prentice-Hall, Upper Saddle River, NJ, 1998).
53. G. S. Boulton and R. C. A. Hindmarsh, *J. Geophys. Res*. **92**, 9059 (1987).
54. B. Kamb, *J. Geophys. Res*. **96**, 16, 585 (1991).
55. R. C. A. Hindmarsh, *Quat. Sci. Rev*. **16**, 1039 (1997).
56. N. R. Iverson *et al*., *J. Glaciol*. **44**, 634 (1998).
57. N. R. Iverson, B. Hanson, R. LeB. Hooke, P. Jansson, *Science* **267**, 80 (1995); N. R. Iverson, *J. Glaciol*. **45**, 41 (1999).
58. S. J. Marshall, L. Tarasov, G. K. C. Clarke, W. R. Peltier, *Can J. Earth Sci*., in press.
59. T. J. Hughes, *Rev. Geophys*. **13**, 502 (1975).
60. D. D. Blankenship, C. R. Bentley, S. T. Rooney, R. B. Alley, *Nature* **322**, 54 (1986); S. Anandakrishnan and R. B. Alley, *J. Geophys. Res*. **102**, 15, 183 (1997).
61. H. Engelhardt, N. Humphrey, B. Kamb, M. Fahnestock, *Science* **248**, 57 (1990).
62. S. J. Marshall, G. K. C. Clarke, A. S. Dyke, D. A. Fisher, *J. Geophys. Res*. **101**, 17, 827 (1996).
63. N. G. Pisias and T. C. Moore Jr., *Earth Planet. Sci. Lett*. **52**, 450 (1981).
64. P. B. deMenocal, *Science* **270**, 53 (1995).
65. D. F. Williams *et al*., *Science* **278**, 1114 (1997).
66. S. C. Clemens, D. W. Murray, W. L. Prell, *Science* **274**, 943 (1996).
67. Z. Ding, Z. Yu, N. W. Rutter, T. Liu, *Quat. Sci. Rev*. **13**, 39 (1994).
68. J. Oerlemans, in *Milankovitch and Climate, Part 2*, A. L. Berger *et al*., Eds. (D. Reidel, Norwell, MA, 1984), pp. 607–611; B. Saltzman and K. A. Maasch, *Clim. Dyn*. **5**, 201 (1991); A. Berger, X. S. Li, M. F. Loutre, *Quat. Sci. Rev*. **18**, 1 (1999).
69. D. Paillard, *Nature* **391**, 378 (1998).
70. G. DeBlonde and W. R. Peltier, *J. Clim*. **4**, 318 (1991); M. Mudelsee and M. Schulz, *Earth Planet. Sci. Lett*. **151**, 117 (1997).
71. Muller and MacDonald [R. A. Muller and G. J. MacDonald, *Science* **277**, 215 (1997)] argued that the origin of the 100-ky cycle involves non-Milankovitch changes in the Earth's orbital inclination, which caused the Earth to periodically pass through a cloud of interplanetary dust. Sedimentary records and calculations of dust flux, however, do not show large changes in extraterrestrial dust accretion [F. Marcantonio *et al*., *Nature* **383**, 705 (1996); F. Marcantonio *et al*., *Earth Planet. Sci. Lett*. **170**, 157 (1999); S. J. Kortenkamp and S. F. Dermott, *Science* **280**, 874 (1998)], whereas spectral analyses of the marine $\delta^{18}O$ record of global ice volume suggest that this mechanism is unnecessary [J. A. Rial, *Science* **285**, 564 (1999); A. J. Ridgwell, A. J. Watson, M. E. Raymo, *Paleoceanography* **14**, 437 (1999)].
72. W. S. Broecker and J. van Donk, *Rev. Geophys. Space Phys*. **8**, 169 (1970).
73. W. T. Hyde and W. R. Peltier, *J. Atmos. Sci*. **42**, 2170 (1985).
74. L. Tarasov and W. R. Peltier, *J. Geophys. Res*. **104**, 9517 (1999).
75. J. Mangerud, in *Quaternary Landscapes*, L. K.C. Shane and E. J. Cushing, Eds. (Univ. of Minnesota Press, Minneapolis, 1991), pp. 38–75; P. U. Clark *et al*., *Quat. Sci. Rev*. **12**, 79 (1993).
76. W. R. Peltier, *Rev. Geophys*. **36**, 603 (1998).
77. S. J. Marshall, thesis, University of British Columbia (1996).
78. W. S. Broecker, *Paleoceanography* **13**, 119 (1998).
79. R. B. Alley, P. U. Clark, L. D. Keigwin, R. S. Webb, in *Mechanisms of Global Climate Change at Millennial Time Scales*, P. U. Clark, R. S. Webb, L. D. Keigwin, Eds. (AGU, Washington, DC, 1999), pp. 385–394.
80. W. S. Broecker *et al*., *Nature* **341**, 318 (1989); P. U. Clark *et al*., *Paleoceanography* **11**, 563 (1996); D. C. Barber *et al*., *Nature* **400**, 344 (1999); J. M. Licciardi, J. T. Teller, P. U. Clark, in *Mechanisms of Global Climate Change at Millennial Time Scales*, P. U. Clark, R. S. Webb, L. D. Keigwin, Eds. (AGU, Washington, DC, 1999), pp. 177–200; S. J. Marshall and G. K. C. Clarke, *Quat. Res*., in press.
81. M. A. Cane and A. C. Clement, in *Mechanisms of Global Climate Change at Millennial Time Scales*, P. U. Clark, R. S. Webb, L. D. Keigwin, Eds. (AGU, Washington, DC, 1999), pp. 373–384.
82. L. D. Keigwin and S. J. Lehman, *Paleoceanography* **9**, 185 (1994); W. B. Curry, T. M. Marchitto, J. F. McManus, D. W. Oppo, K. L. Laarkamp, in *Mechanisms of Global Climate Change at Millennial Time Scales*, P. U. Clark, R. S. Webb, L. D. Keigwin, Eds. (AGU, Washington, DC, 1999), pp. 59–76.
83. S. J. Marshall and G. K. C. Clarke, *J. Geophys. Res*. **102**, 17827 (1997).
84. COHMAP Members, *Science* **241**, 1043 (1988); S. Pinot *et al*., *Clim. Dyn*., in press.
85. E. Bard, *Science* **284**, 1133 (1999).
86. W. R. Peltier, *Science* **265**, 195 (1994).
87. K. Lambeck, C. Smither, P. Johnston, *Geophys. J. Int*. **134**, 102 (1998).
88. CLIMAP Project Members, *Geol. Soc. Am. Map Chart Ser. 36* (1981).
89. P. Huybrechts and S. T'Siobbel, *Ann. Glaciol*. **25**, 333 (1997).
90. R. B. Alley, *J. Glaciol*. **38**, 245 (1992).
91. R. H. Thomas, *J. Glaciol*. **12**, 55 (1973); K. C. Jezek, R. B. Alley, R. H. Thomas, *Science* **227**, 1335 (1985).
92. G. S. Boulton, G. D. Smith, A. S. Jones, J. Newsome, *J. Geol. Soc. London* **142**, 447 (1985).
93. D. A. Fisher, N. Reeh, K. Langley, *Geophys. Phys. Quat*. **39**, 229 (1985).
94. P. U. Clark, J. M. Licciardi, D. R. MacAyeal, J. W. Jenson, *Geology* **24**, 679 (1996).
95. J. M. Licciardi, P. U. Clark, J. W. Jenson, D. R. MacAyeal, *Quat. Sci. Rev*. **17**, 427 (1998).
96. J. X. Mitrovica and J. L. Davis, *Earth Planet. Sci. Lett*. **136**, 343 (1995); J. L. Davis and J. X. Mitrovica, *Nature* **379**, 331 (1996).
97. N. G. Pisias and A. C. Mix, *Paleoceanography* **12**, 381 (1997); S. E. Harris and A. C. Mix, *Quat. Res*. **51**, 14 (1999).
98. C. Genthon *et al*., *Nature* **329**, 414 (1987); S. M. Colman *et al*., *Nature* **378**, 769 (1995); J. J. Morley and L. E. Heusser, *Paleoceanography* **12**, 483 (1997).
99. P. M. Grootes, M. Stuiver, J. W. C. White, S. J. Johnsen, J. Jouzel, *Nature* **366**, 552 (1993).
100. K. M. Cuffey *et al*., *Science* **270**, 455 (1995); J. P. Severinghaus, T. Sowers, E. J. Brook, R. B. Alley, M. L. Bender, *Nature* **393**, 141 (1998).
101. A. Berger and M. F. Loutre, *Quat. Sci. Rev*. **10**, 297 (1991).
102. H. Schulz, U. von Rad, H. Erlenkeuser, *Nature* **393**, 54 (1998).
103. M. G. Little *et al*., *Paleoceanography* **12**, 568 (1997).
104. S. J. Johnsen, W. Dansgaard, H. B. Clausen, C. C. Langway Jr., *Nature* **235**, 429 (1972).
105. E. J. Brook, personal communication.
106. T. Blunier *et al*., *Nature* **394**, 739 (1998).
107. E. J. Brook, T. Sowers, J. Orchardo, *Science* **273**, 1087 (1996).
108. G. K. C. Clarke *et al*., in *Mechanisms of Global Climate Change at Millennial Time Scales*, P. U. Clark, R. S. Webb, L. D. Keigwin, Eds. (AGU, Washington, DC, 1999), pp. 243–262.
109. T. Sowers and M. Bender, *Science* **269**, 210 (1995).
110. K. Fleming *et al*., *Earth Planet. Sci. Lett*. **163**, 327 (1998).
111. A. Berger, *Quat. Res*. **9**, 139 (1978).
112. Evolutive spectral analyses were calculated by using fast Fourier transform, and spectra were smoothed with a Hanning filter with a half-filter with five spectral estimates. Time series were interpolated to a constant sampling interval and then normalized to a mean zero and a standard deviation of one. Sampling interval was 1 ky for (Fig. 7A) and (Fig. 7D), 2 ky for (Fig. 7E), and 4 ky for (Fig. 7B, C, and F). Every spectrum was calculated with a record length of 1 My with a 100-ky offset. Each 1-My long segment was linearly detrended. Spectra are plotted at the midpoint of each interval, with the first 100-ky interval beginning at 500 ka. Spectral estimates have 15 degrees of freedom.
113. B. K. Linsley, *Nature* 380, **234** (1996).
114. J. Chappell and N. J. Shackleton, *Nature* **324**, 137 (1986); J. Chappell *et al*., *Earth Planet. Sci. Lett*. **141**, 227 (1996).
115. E. Bard, B. Hamelin, R. G. Fairbanks, *Nature* **346**, 456 (1990).

116. We thank T. Blunier, E. Brook, S. Clemens, P. deMenocal, K. Fleming, B. Linsley, A. Mix, J. Peck, H. Schulz, and D. Williams for providing data; P. Bartlein, J. Clark, S. Hostetler, J. Jenson, S. Marshall, D. MacAyeal, A. Mix, and N. Pisias for discussions; P. Bartlein, S. Hostetler, A. Mix, and two external reviewers for reviews; and P. Bartlein, S. Marshall, A. Mix, and N. Pisias for preparing figures. Supported by grants from the Earth System History program (R.B.A., P.U.C., D.P.) and the Office of Polar Programs (R.B.A.) of the NSF.